Non-Adiabatic Transition in Spin-Boson Model and Generalization of the Landau-Zener Formula

Hiroto Kobayashi¹

Department of Physics, Graduate School of Science, University of Tokyo Hongo, Bunkyo-ku, Tokyo 113-0033, Japan

Naomichi Hatano

Theoretical Division, MS-B262, Los Alamos National Laboratory Los Alamos, New Mexico 87545, USA

Seiji Miyashita

Department of Earth and Space Science, Faculty of Science, Osaka University Toyonaka, Osaka 560-0043, Japan

Abstract

Non-adiabatic transitions are studied in a spin-boson model with multiple scattering points. In order to generalize the Landau–Zener formula, which describes the case of a single scattering point, we define an "effective gap" for a set of scattering points. The generalized formula agrees very well with numerical results of the nonadiabatic dynamics, which we obtained by a direct numerical method. This will make the Landau-Zener formula yet more useful in analyzing experimental data of magnetic-moment inversion.

Key words: Landau-Zener formula, quantum dynamics, spin-boson model, exponential product formula

PACS: 05.70.Ln, 05.30.-d, 75.10.Jm, 75.90.+w

Present address: c/o Prof. A. Kuniba, Institute of Physics, University of Tokyo, Komaba, Meguro-ku, Tokyo 153-8902, Japan; Tel.: (+81)-3-5454-4372; e-mail: hiroto@shpb.c.u-tokyo.ac.jp.

1 Introduction

Macroscopic quantum tunneling [1–4] has been an intriguing subject for several years. A few experiments have been carried out [1,4] for mesoscopic magnetic systems in order to determine the coupling matrix element (or the gap) between the two macroscopic states. The basic assumption in analysis of the experimental data is the system Hamiltonian of the form

$$\mathcal{H} = \frac{1}{2}\hbar\delta\sigma^x - \frac{1}{2}H\sigma^z,\tag{1.1}$$

where the up-spin state $|\uparrow\rangle$ and the down-spin state $|\downarrow\rangle$ denote the two macroscopic states, while $\delta(>0)$ in the first term denotes the coupling matrix element between the two states. The coupling $\hbar\delta$ is also called the gap, the reason of which is obvious in the schematic energy spectrum in Fig. 1.

The major experimental method of measuring the gap $\hbar\delta$ is to apply an oscillating field to the system and seek resonance due to the gap at H=0. However, this method may pick resonance of various other degrees of freedom in real materials and mix them up with the resonance due to the gap [2]. Hence, one of the present authors [5] suggested applying a constantly changing field instead of an oscillatory field and estimating the coupling $\hbar\delta$ by the use of the Landau–Zener formula [7,8].

Suppose that the system is first under a large field in the negative direction $(H \ll -\hbar \delta)$ and the spin is approximately in the down-spin state. If the field is switched to the positive direction very slowly, or adiabatically, the system follows the ground state and eventually converges to the up-spin state for $H \gg \hbar \delta$; thus the spin is flipped. If the field is changed more rapidly, however, the system does not necessarily follow the ground state and may remain in the down-spin branch even after the field becomes positive. In other words, the system is excited to the higher energy level at H = 0 with a certain probability p. This phenomenon is called non-adiabatic transition. Hereafter, we refer to the point where the transition takes place as the scattering point. In this case, the scattering point is H = 0.

The Landau–Zener theory [7,8] gives the "passing" probability p in the following form:

$$p = \exp\left[-\frac{\pi}{2\hbar}(\Delta E)^2 v^{-1}\right]. \tag{1.2}$$

Thus the spin is flipped with the probability 1-p. Here ΔE is the gap at the scattering point; hence $\Delta E = \hbar \delta$ in the case of Eq. (1.1). The parameter v

denotes the rate of the field change; that is, the field is increased from a large-magnitude negative value to a large positive value as H(t) = vt, where t is the time. Hence, to measure the flipping probability under a constantly changing field should give an estimate of the gap $\hbar\delta$ from Eq. (1.2) [5], provided that the above Hamiltonian (1.1) approximates experimental systems well.

In real materials, however, there must be always coupling between the magnetic moment and phonons. Hence, in the present paper, we study non-adiabatic transitions in the following spin-boson model [9]:

$$\mathcal{H} = -\frac{1}{2}\hbar\delta\sigma^x - \frac{1}{2}H(t)\sigma^z + \sum_{\alpha}\hbar\omega_{\alpha}\left(n_{\alpha} + \frac{1}{2}\right) + \sum_{\alpha}V_{\alpha}\sigma^z(b_{\alpha}^{\dagger} + b_{\alpha}). \quad (1.3)$$

The third term denotes various phonon modes and the fourth term denotes the coupling between the spin and the phonons. As we show below, the energy spectrum of the model (1.3) have many scattering points at various values of H. The main purpose of the present paper is to show how we should modify the Landau–Zener theory for such a problem. To generalize the formula (1.2) to multiple-scattering cases, we introduce a new parameter, the effective gap. The effective gap, when it replaces the gap ΔE in the Landau–Zener formula (1.2), explains well the multiple-scattering data which we numerically calculated using the exponential product formula [10,11].

If the scattering points are well separated from each other in the energy spectrum, a non-adiabatic transition at *each* scattering point can be regarded as an independent event and should be well approximated by the Landau–Zener formula (1.2). We can explain the entire time evolution as a simple sequence of these independent events. This is the case if the model (1.3) has only one boson mode. We first consider this case in Sec. 2 and show that the Landau–Zener formula is indeed consistent with the numerical results.

However, this naive description should fail if some of the scattering points are close to each other. This situation arises when we consider multiple boson modes. We show in Sec. 3 that the numerical results in two-mode cases can be well parametrized with a single parameter, namely, the effective gap.

For numerical calculations of the dynamics of the system, we changed the magnetic field from $-H_{\text{max}}$ to H_{max} in the time range $-t_{\text{max}} \leq t \leq t_{\text{max}}$; hence the rate of the field change is $v = H_{\text{max}}/t_{\text{max}}$ and the change schedule is

$$H(t) = vt = \frac{H_{\text{max}}}{t_{\text{max}}} t \quad \text{for} \quad -t_{\text{max}} \le t \le t_{\text{max}}.$$
 (1.4)

We made the maximum field strength H_{max} much greater than $\hbar\delta$ to ensure that the numerical results well approximate the non-adiabatic dynamics with

 $H_{\rm max}=\infty$. We calculated the time evolution of the system, taking the ground state for $H=-H_{\rm max}$ as the initial state. Further computational details are given in Appendix.

Incidentally, we hereafter use dimensionless parameters for simplicity, taking $H_{\rm max}$ as the unit of energy. A tilde mark on top of each parameter indicates that the parameter is dimensionless: e.g. $\tilde{\mathcal{H}} \equiv \mathcal{H}/H_{\rm max}$, $\tilde{\delta} \equiv \hbar \delta/H_{\rm max}$, $\tilde{\omega}_{\alpha} \equiv \hbar \omega_{\alpha}/H_{\rm max}$, $\tilde{V}_{\alpha} \equiv V_{\alpha}/H_{\rm max}$, $\tilde{H}(\tilde{t}) \equiv H(t)/H_{\rm max}$, and $\tilde{t} \equiv tH_{\rm max}/\hbar$. Hence the Hamiltonian (1.3) now reads

$$\tilde{\mathcal{H}} = -\frac{1}{2}\tilde{\delta}\sigma^x - \frac{1}{2}\tilde{H}(\tilde{t})\sigma^z + \sum_{\alpha}\tilde{\omega}_{\alpha}\left(n_{\alpha} + \frac{1}{2}\right) + \sum_{\alpha}\tilde{V}_{\alpha}\sigma^z(b_{\alpha}^{\dagger} + b_{\alpha}) \quad (1.5)$$

with the field-change schedule given by

$$\tilde{H}(\tilde{t}) = \tilde{v}\tilde{t}$$
 with $\tilde{v} = \frac{\hbar}{H_{\text{max}}^2} v = \frac{1}{\tilde{t}_{\text{max}}}$ for $-\tilde{t}_{\text{max}} \le \tilde{t} \le \tilde{t}_{\text{max}}$. (1.6)

In this dimensionless notation, the maximum field is $\tilde{H}_{max}=1$. The Landau–Zener formula reads

$$p = \exp\left[-\frac{1}{2}\pi(\Delta\tilde{E})^2\tilde{v}^{-1}\right]. \tag{1.7}$$

2 Non-Adiabatic Transition and the Landau–Zener Formula

In the present section, we treat the spin-boson model with a single boson mode. We calculate time evolution from the initial state and analyze it with the Landau–Zener formula.

The energy spectrum of the Hamiltonian (1.5) is exemplified in Fig. 2, showing its dependence on \tilde{H} . (Note that the spectrum is calculated for each fixed value of \tilde{H} , not under a changing field $\tilde{H}(\tilde{t})$.) The values of the Hamiltonian parameters are fixed to

$$\tilde{\delta} = 0.05, \quad \tilde{\omega}_1 = 0.3, \quad \text{and} \quad \tilde{V}_1 = \frac{0.1}{\sqrt{0.3}}$$
 (2.1)

throughout this section. (The reason of the seemingly strange choice of \tilde{V}_1 is that the spin-boson coupling \tilde{V}_{α} often scales as $1/\sqrt{\tilde{\omega}_{\alpha}}$.)

In Fig. 2, the states with positive slopes have a large component of the spindown state, while those with negative slopes have a large component of the spin-up state. The states with the same spin but different energies differ in the approximate number of excited bosons. (These interpretations are indicated in Fig. 2.) The initial state, which is the ground state for $H = -H_{\text{max}}$, or $\tilde{H} = -1$, is hence approximately a spin-down state without any bosons. As \tilde{H} is increased at a finite rate \tilde{v} , the state evolves along the ground state of the Hamiltonian before it encounters a nearly degenerate state at the scattering point at $\tilde{H} = 0$. Non-adiabatic transitions occur afterward.

For example, the magnetization of the spin $\langle \sigma^z \rangle_{\tilde{t}}$ and the total energy $\tilde{E}(\tilde{t}) = \langle \tilde{\mathcal{H}} \rangle_{\tilde{t}}$ evolve as shown in Fig. 3 when the magnetic field is increased as scheduled in Eq. (1.6) with $\tilde{v} = 1/500$. Here the angle brackets $\langle \cdots \rangle_{\tilde{t}}$ denote the expectation value with respect to the wave function at time \tilde{t} : $\langle \Psi(\tilde{t}) | \cdots | \Psi(\tilde{t}) \rangle$. (See Appendix for details of the computation.) The initial state (approximately $|\downarrow,0\rangle$) is scattered when it passes the scattering point at $\tilde{H}=0$. The resulting state for $0 \lesssim \tilde{t} \lesssim 0.3 \ \tilde{t}_{\rm max}$ is a superposition of the ground state (approximately $|\uparrow,0\rangle$) and the first-excited state (approximately $|\downarrow,0\rangle$). Hence the magnetization is not fully inverted at $\tilde{H}=0$. (The oscillation of the magnetization after the non-adiabatic transition is due to the spin precession. This becomes evident when we see that the energy of the spin does not change as rapidly as the magnetization does; see Fig. 4.)

The above explanation is supported by the time-evolution data of the eigenstate weights p_i , where each p_i denotes the weight of the (i-1)th excited state in the evolving state $\Psi(\tilde{t})$. In other words, we define the weights by $p_i(\tilde{t}) = |w_i(\tilde{t})|^2$, where we expand the evolving state $\Psi(\tilde{t})$ with respect to the eigenfunctions $\{\phi_i(\tilde{H}(\tilde{t}))\}$ of the Hamiltonian at time \tilde{t} as follows:

$$\Psi(\tilde{t}) = \sum_{i} w_i(\tilde{t})\phi_i(\tilde{H}(\tilde{t})). \tag{2.2}$$

The result of the calculation for the present case is shown in Fig. 5. The state $\Psi(\tilde{t})$ for $0 \lesssim \tilde{t} \lesssim 0.3 \ \tilde{t}_{\text{max}}$ is the superposition of the two states $|\uparrow,0\rangle$ and $|\downarrow,0\rangle$, as is expected.

As the applied field is increased further from $\tilde{H}=0$, the component p_2 of the evolving state $\Psi(\tilde{t})$ undergoes a subsequent non-adiabatic transition around $\tilde{t}=0.3$ \tilde{t}_{\max} and spawns the component p_3 . The component $p_2(\tilde{t})$ for 0.3 $\tilde{t}_{\max}\lesssim \tilde{t}\lesssim 0.6$ \tilde{t}_{\max} corresponds to $|\uparrow,1\rangle$, a spin-up state with one boson emitted, while the spawned component $p_3(\tilde{t})$ in the same time range is approximately $|\downarrow,0\rangle$. The component p_3 undergoes further non-adiabatic transitions afterward. Thus the final state for $\tilde{t}=\infty$ will be a superposition of spin-up states with various numbers of bosons.

In this one-mode case, the scattering points are far apart from each other. We then expect that the whole event is regarded as a series of independent non-adiabatic transitions, each of which can be treated by the Landau–Zener formula (1.7). Hence the passing probability after the transition at the scattering point $\tilde{H}=0$ should be

$$p_2(\tilde{t}) = \exp\left[-\frac{1}{2}\pi(\Delta \tilde{E}_1)^2 \tilde{v}^{-1}\right] \quad \text{for} \quad 0 \lesssim \tilde{t} \lesssim 0.3 \ \tilde{t}_{\text{max}},\tag{2.3}$$

while the probability that the state remains in the lower level is $p_1 = 1 - p_2$. Here $\Delta \tilde{E}_1$ corresponds to the energy gap between the ground and the first excited states at $\tilde{H} = 0$. Similarly for the subsequent non-adiabatic transition around $\tilde{t} = 0.3$ \tilde{t}_{max} , the passing probability is given by $\exp[-\frac{1}{2}\pi(\Delta \tilde{E}_2)^2\tilde{v}^{-1}]$, where $\Delta \tilde{E}_2$ is the energy gap between the first and second excited states at the scattering point. The passing probability for the set of the two scattering points with the gaps $\Delta \tilde{E}_1$ and $\Delta \tilde{E}_2$ should be given by

$$p_{3}(\tilde{t}) = \exp\left[-\frac{1}{2}\pi(\Delta\tilde{E}_{1})^{2}\tilde{v}^{-1}\right] \exp\left[-\frac{1}{2}\pi(\Delta\tilde{E}_{2})^{2}\tilde{v}^{-1}\right]$$

$$= \exp\left\{-\frac{1}{2}\pi\left[(\Delta\tilde{E}_{1})^{2} + (\Delta\tilde{E}_{2})^{2}\right]\tilde{v}^{-1}\right\}$$
for $0.3 \ \tilde{t}_{\max} \lesssim \tilde{t} \lesssim 0.6 \ \tilde{t}_{\max}$. (2.4)

On the other hand, the probability of the first excited component in this time range is

$$p_2(\tilde{t}) = \exp\left[-\frac{1}{2}\pi(\Delta \tilde{E}_1)^2 \tilde{v}^{-1}\right] \left\{1 - \exp\left[-\frac{1}{2}\pi(\Delta \tilde{E}_2)^2 \tilde{v}^{-1}\right]\right\}$$
for $0.3 \ \tilde{t}_{\text{max}} \lesssim \tilde{t} \lesssim 0.6 \ \tilde{t}_{\text{max}}.$ (2.5)

We can continue the calculation for subsequent transitions.

Indeed, the above theoretical argument explains our numerical data of the magnetization very well, as is shown in Fig. 6. Thus we can in turn estimate the energy gap of each scattering point from the time dependence of the magnetization [5,6].

However, we cannot naively apply the Landau–Zener theory to cases where some of the scattering points lie closely to each other. This is the central issue of Sec. 3. Before we proceed to the next section, a remark on Eq. (2.4) is in order; the expression can be formally regarded as if the system underwent one non-adiabatic transition at a single scattering point with an "effective gap" $\Delta \tilde{E}^{(\text{eff})}$ defined in

$$\left(\Delta \tilde{E}^{(\text{eff})}\right)^2 = \left(\Delta \tilde{E}_1\right)^2 + \left(\Delta \tilde{E}_2\right)^2,\tag{2.6}$$

as has been pointed out by Kayanuma [12]. We show in the next section that the passing probability can be written in the Landau–Zener form with an effective gap even when scattering points are close to each other, although the value of the effective gap can be different from the one given in Eq. (2.6).

3 Successive Non-Adiabatic Transitions and Effective Gap

In the present section, we consider the spin-boson model with two boson modes. We discuss the case where non-adiabatic transitions cannot be regarded as independent events. We introduce the effective gap to generalize the Landau–Zener formula to such a case. We study how the magnitude of the effective gap depends on the distance between two scattering points.

In this section we keep the first boson mode the same as in Eq. (2.1) and change the parameters of the second boson mode as follows:

- (i) $\tilde{\omega}_2 = 0.35$ and $\tilde{V}_2 = 0.1/\sqrt{0.35}$;
- (ii) $\tilde{\omega}_2 = 0.31$ and $\tilde{V}_2 = 0.1/\sqrt{0.31}$; (iii) $\tilde{\omega}_2 = \tilde{\omega}_1 = 0.3$ and $\tilde{V}_2 = \tilde{V}_1 = 0.1/\sqrt{0.3}$.

We calculated the system dynamics, again taking the ground state for H = -1as the initial condition.

In the case (i), there are two scattering points quite close but still apart. We show that the passing probability for this case can be given by the product of two passing probabilities with the real values of the energy gaps.

This is not true in the case (ii), where the two scattering points are much closer than in the case (i). However, we show numerically that the same formula of the passing probability is still applicable, although we have to replace the real values of the gaps with an effective gap. (In fact, the real energy gaps are not clearly defined in the case (ii) anymore.) The remarkable point is that the single parameter of the effective gap determines the passing probabilities for various field-change rates. This is a non-trivial observation.

In the case (iii), the two modes are degenerate and the two scattering points in question are reduced to one point. Then the original single-scattering Landau-Zener formula becomes applicable again, but with a single real energy gap instead of two gaps.

We then show in the last subsection that the effective gap estimated in the case (ii) smoothly interpolates the real energy gaps in the cases (i) and (iii). Thus we conclude that the effective gap is a very useful concept in analyzing numerical and experimental data.

3.1 Case (i)

We show in Fig. 7 the energy spectrum of the spin-boson model with two boson modes in the case (i): $\tilde{\delta} = 0.05$, $\tilde{\omega}_1 = 0.3$, $\tilde{\omega}_2 = 0.35$, $\tilde{V}_1 = 0.1/\sqrt{0.3}$, and $\tilde{V}_2 = 0.1/\sqrt{0.35}$. The time evolution starts with the ground state at $\tilde{H} = -1$ and goes through the scattering points near $\tilde{H} = 0$, 0.3, 0.35,.... We calculated the time evolution of the magnetization $\langle \sigma^z \rangle_{\tilde{t}}$ of the spin and the total energy, as shown in Fig. 8.

Let us focus on the scattering points near $\tilde{H}=0.3$ and 0.35. Although these two are fairly separated, we cannot resolve the magnetization jump around $\tilde{H}=0.3\sim0.35$ into two non-adiabatic transitions. The spin-precession oscillation probably smeared out the two magnetization jumps. Still, we can resolve it into two in the calculations of the eigenstate weights, the same quantities as plotted in Fig. 5. In Fig. 9, we can separate the two "scattering regions," where the eigenstate weights p_i drastically change. Indeed, the values of the eigenstate weights are consistent with the Landau–Zener formulas separately applied to the two scattering points; i.e. the eigenstate weight p_2 converges to

$$p_2 = \exp\left[-\frac{1}{2}\pi(\Delta\tilde{E}_1)^2\tilde{v}^{-1}\right] \left\{1 - \exp\left[-\frac{1}{2}\pi(\Delta\tilde{E}_2)^2\tilde{v}^{-1}\right]\right\}$$
(3.1)

and p_3 to

$$p_{3} = \exp\left[-\frac{1}{2}\pi(\Delta\tilde{E}_{1})^{2}\tilde{v}^{-1}\right] \exp\left[-\frac{1}{2}\pi(\Delta\tilde{E}_{2})^{2}\tilde{v}^{-1}\right] \times \left\{1 - \exp\left[-\frac{1}{2}\pi(\Delta\tilde{E}_{3})^{2}\tilde{v}^{-1}\right]\right\}$$

$$(3.2)$$

for $\tilde{t} = \tilde{t}_{\text{max}}$. Here $\Delta \tilde{E}_1$, $\Delta \tilde{E}_2$, and $\Delta \tilde{E}_3$ are the energy gaps at the scattering points near $\tilde{H} = 0$, 0.3, and 0.35, respectively.

Since the magnetization behaves as if there is a single non-adiabatic transition around $\tilde{H}=0.3\sim0.35$, the situation remarked at the end of the previous section now becomes a reality in terms of the magnetization. That is, the magnetization jump around $\tilde{H}=0.3\sim0.35$ is approximately described by a single Landau–Zener formula (1.7) with the effective gap

$$\left(\Delta \tilde{E}^{(\text{eff})}\right)^2 \simeq \left(\Delta \tilde{E}_2\right)^2 + \left(\Delta \tilde{E}_3\right)^2.$$
 (3.3)

This is plotted in Fig. 8 as a dotted line with steps.

3.2 Case (ii)

If two scattering points lie close within the width of the scattering region, we cannot regard two non-adiabatic transitions as independent events anymore. In the energy spectrum in the case (ii), the scattering points near $\tilde{H} = 0.3$ and 0.31 are so close that we cannot even define the energy gaps $\Delta \tilde{E}_2$ and $\Delta \tilde{E}_3$; see Fig. 10. The time evolution of the eigenstate weights p_i are shown in Fig. 11. We see from this figure that the two non-adiabatic processes are not separate enough to be independent.

In this case, we propose a new definition of the effective gap for the non-adiabatic transitions around $\tilde{H} = 0.3 \sim 0.31$. With this newly defined effective gap $\Delta \tilde{E}^{(\text{eff})}$, the magnetization jump around $\tilde{H} = 0.3 \sim 0.31$ is described by a single Landau–Zener formula; see Fig. 12.

Let us describe the definition of the effective gap in the following. First, we define the effective gap $\Delta \tilde{E}_i^{(\text{eff})}$ for each scattering point with

$$p_i(\tilde{t}_{\text{max}}) = \left[1 - \sum_{j=1}^{i-1} p_j(\tilde{t}_{\text{max}})\right] \left\{1 - \exp\left[-\frac{1}{2}\pi(\Delta \tilde{E}_i^{(\text{eff})})^2 \tilde{v}^{-1}\right]\right\}.$$
(3.4)

Specifically, we obtain the first estimate $\Delta \tilde{E}_1^{(\text{eff})}$ from the value of $p_1(\tilde{t}_{\text{max}})$ as

$$\Delta \tilde{E}_1^{\text{(eff)}} = \sqrt{-\frac{2\tilde{v}}{\pi} \log[1 - p_1(\tilde{t}_{\text{max}})]}.$$
 (3.5)

Since the scattering point at $\tilde{H}=0$ is far apart from the other scattering points, the estimate $\Delta \tilde{E}_1^{(\text{eff})}$ simply coincides with the real gap $\Delta \tilde{E}_1$ between the ground and first excited states at $\tilde{H}=0$. The second estimate $\Delta \tilde{E}_2^{(\text{eff})}$ is given by

$$p_2(\tilde{t}_{\text{max}}) = \left[1 - p_1(\tilde{t}_{\text{max}})\right] \left\{1 - \exp\left[-\frac{1}{2}\pi(\Delta \tilde{E}_2^{(\text{eff})})^2 \tilde{v}^{-1}\right]\right\},$$
 (3.6)

or

$$\Delta \tilde{E}_2^{\text{(eff)}} = \sqrt{-\frac{2\tilde{v}}{\pi} \log \left[1 - \frac{p_2(\tilde{t}_{\text{max}})}{1 - p_1(\tilde{t}_{\text{max}})} \right]}.$$
 (3.7)

This effective gap, however, has no counterpart to be compared with, since we cannot properly define the energy gap between the first and second excited states at the scattering point near $\tilde{H}=0.3$. This is also the case for the third

estimate $\Delta \tilde{E}_3^{(\text{eff})}$. By adding the last two effective gaps squared, we then define the combined effective gap $\Delta \tilde{E}^{(\text{eff})}$ for the transitions around $\tilde{H} = 0.3 \sim 0.31$:

$$\left(\Delta \tilde{E}^{(\text{eff})}\right)^2 = \left(\Delta \tilde{E}_2^{(\text{eff})}\right)^2 + \left(\Delta \tilde{E}_3^{(\text{eff})}\right)^2. \tag{3.8}$$

The dotted line with steps in Fig. 12 was drawn, using the Landau–Zener formula with the above combined effective gap.

The key point here is that thus-defined effective gaps barely depend on the field-change rate \tilde{v} ; see Fig. 13. (Otherwise the definition of the effective gaps would be just a transformation of the eigenstate weights.) Therefore, once we estimate the effective gaps for one particular value of \tilde{v} , we can predict the magnetization jump for arbitrary values of \tilde{v} . This is the central point of the present paper.

3.3 Case (iii)

The energy spectrum in the case (iii), $\omega_1 = \omega_2 = 0.3$, is shown in Fig. 14. The two scattering points around $\tilde{H} = 0.3$ are now reduced to one. In this case, the second excited state at the scattering point near $\tilde{H} = 0.3$ is not coupled to either the first or the third excited states [12]. This is demonstrated in Fig. 15; the component of the second excited state, p_3 , entirely vanishes. Since the second excited state becomes irrelevant near $\tilde{H} = 0.3$, the non-adiabatic transition there occurs only between the first and the third excited states. Thus we recover the original Landau–Zener problem for two states. The time dependence of the magnetization is well explained by the Landau–Zener formula with the irrelevant states neglected. The magnetization jump around $\tilde{H} = 0.3$ is given by the formula (1.7) with the real energy gap between the first and the third excited states (the dotted line with steps in Fig. 16).

3.4 Effective gap and separation of two scattering points

We have shown above that the case (i) and the case (iii) are explained by the original Landau–Zener theory for a single non-adiabatic transition between two states. The passing probabilities are fully described by the formula (1.7) with the real values of the energy gaps at the scattering points. In the intermediate region including the case (ii), on the other hand, we need to use the effective gap for the formula, since the real energy gaps are not clearly defined. We here show that the effective gap estimated in the intermediate region smoothly interpolates the real energy gaps in the limiting cases (i) and (iii).

We calculated the effective gap in the intermediate region, fixing $\tilde{\omega}_1 = 0.3$ and changing $\tilde{\omega}_2$ in the range $0.3 \leq \tilde{\omega}_2 \leq 0.35$. (We changed \tilde{V}_2 at the same time so that $\tilde{V}_2 \propto 1/\sqrt{\tilde{\omega}_2}$.) By varying the value of $\tilde{\omega}_2$, we change the separation of the two scattering points around $\tilde{H} \sim 0.3$. Figure 17 shows the $\tilde{\omega}_2$ -dependence of the effective gaps $\Delta \tilde{E}_1^{(\text{eff})}$, $\Delta \tilde{E}_2^{(\text{eff})}$, and $\Delta \tilde{E}_3^{(\text{eff})}$, which are defined in Eq. (3.4). We can see that the effective gaps in the intermediate region smoothly interpolate the two cases (i) and (iii). This shows that the data analysis with the effective gap is very stable.

To put the above in another perspective, we show in Fig. 18 the discrepancy between the real energy gap and the effective energy gap. In the case (i), the effective gap $\Delta \tilde{E}^{(\text{eff})}$ is approximately given by the real energy gaps as in Eq. (3.3), or

$$\left(\Delta \tilde{E}^{(\text{eff})}\right)^2 \simeq \left(\Delta \tilde{E}_2\right)^2 + \left(\Delta \tilde{E}_3\right)^2.$$
 (3.9)

We can see in Fig. 18 that the discrepancy at $\tilde{\omega}_2 = 0.35$ is only about 2%. Although the real energy gaps may not be clearly defined in the intermediate region $0.3 \leq \tilde{\omega}_2 \leq 0.35$, let us, only for illustration purposes, define (a) $\Delta \tilde{E}_2$ as the energy difference between the first and the second excited states at $\tilde{H} = \tilde{\omega}_1 = 0.3$ and (b) $\Delta \tilde{E}_3$ as the energy difference between the second and the third excited states at $\tilde{H} = \tilde{\omega}_2$. The right-hand side of Eq. (3.9) thus estimated (the dashed line in Fig. 18) becomes apart from the effective gap when the two scattering points get close to each other as $\tilde{\omega}_2 \to \tilde{\omega}_1$. Note that it is the effective gap, not the real gaps, that describes the dynamics correctly.

In the case (iii), the real gaps tentatively defined as above is now related to the effective energy gap as $\Delta \tilde{E}^{(\text{eff})} = \Delta \tilde{E}_2 + \Delta \tilde{E}_3$. The left-hand side squared is the dotted line in Fig. 18. This becomes apart from the effective gap when the two scattering points get separated from each other. Figure 18 also shows that the effective gap is a useful way of interpolating the two limiting cases.

4 Summary

In the present paper, we studied the time evolution of a spin-boson model which may be relevant to systems with macroscopic quantum tunneling. We introduced the definition of the effective gap to explain multiple non-adiabatic transitions in complicated energy spectra. With the use of the effective gap, the Landau–Zener formula, originally obtained for a single scattering point, explains the model's multiple magnetization jumps. The important point is that the effective gap estimated in one case of time evolution (i.e. for one value of \tilde{v}) predicts the dynamics for all other values of \tilde{v} . This fact will make

the Landau–Zener formula yet more useful in analyzing experimental data of magnetic-moment inversion.

We remark on a related work on multiple non-adiabatic transitions. Kayanuma and Fukuchi [12] studied successive non-adiabatic transitions in the following generalized case which consists of assembly of the Landau–Zener scattering points:

$$\mathcal{H}(t) = \begin{pmatrix} vt & J_1 & J_2 & J_3 & \cdots \\ J_1 & \varepsilon_1 & & 0 \\ J_2 & & \varepsilon_2 & \\ J_3 & & & \varepsilon_3 \\ \vdots & 0 & & \ddots \end{pmatrix}. \tag{4.1}$$

Here the parameters v, $\{\varepsilon_i\}$, and $\{J_i\}$ are arbitrary constants. The theory concludes that the overall passing probability is given by

$$P = \exp\left(-\frac{2\pi}{\hbar} \sum_{i} J_i^2 |v|^{-1}\right) \tag{4.2}$$

for arbitrary values of $\{\varepsilon_i\}$.

The energy spectrum of the above Hamiltonian appears quite similar to the energy spectra of the present spin-boson model, particularly when $\frac{1}{2}vt$ is subtracted from all the diagonal elements of the Hamiltonian (4.1). In fact, consider the case where all the off-diagonal couplings $\{J_i\}$ are much smaller than the level spacings of $\{\varepsilon_i\}$. The structure of the energy spectrum is almost equivalent to the energy spectrum in Fig. 2 except for the levels $|\downarrow, n>0\rangle$ (which do not contribute to the dynamics in any case). Then the correspondence $\Delta E_i = 2J_i$ becomes evident.

To put it in other words, comparison of our conclusion with Eq. (4.2) leads us to the speculation that our spin-boson model may be reduced to an effective Hamiltonian of the form

$$\mathcal{H}^{(\text{eff})} = \begin{pmatrix} H(t) & \frac{1}{2}\Delta E_1^{(\text{eff})} & \frac{1}{2}\Delta E_2^{(\text{eff})} & \cdots \\ \frac{1}{2}\Delta E_1^{(\text{eff})} & \varepsilon_1 & & 0 \\ \frac{1}{2}\Delta E_2^{(\text{eff})} & & \varepsilon_2 & \\ \vdots & 0 & & \ddots \end{pmatrix} - \frac{1}{2}H(t). \tag{4.3}$$

However, the reduction procedure, if any, is yet to be known.

Finally, the exponential product formula reviewed in Appendix has proven very useful in calculating non-adiabatic dynamics accurately. We hope the formula plays an important role for many problems of quantum dynamics in systems with more complicated interactions.

A Exponential Product Formula for Time-Dependent Hamiltonians

In this Appendix we review the computational method employed in the present paper, namely the exponential product formula [10].

In our previous study [11], we discussed the time evolution of the spin-boson model (1.3) in a constant magnetic field using the exponential product formula. In this case, the diagonalization, if possible, of the Hamiltonian might suffice to know the dynamics. In non-adiabatic transitions, on the other hand, diagonalization of the Hamiltonian does not provide enough information for computation of its quantum dynamics, because of the time dependence of the Hamiltonian. Since quantities change dramatically when the system undergoes non-adiabatic transition, high precision is required to calculations of the time evolution; even small computational errors near the transition points can result in large errors at later stages of the time evolution. The exponential product formula is indispensable in such problems.

When the Hamiltonian depends on time explicitly, a formal solution of the Schrödinger equation

$$i\hbar \frac{\partial}{\partial t} \Psi(t) = \mathcal{H}(t)\Psi(t)$$
 (A.1)

is given by $\Psi(t) = U(t,0)\Psi(0)$, where U(t,0) is the following time-ordered exponential:

$$U(t,0)$$

$$= \operatorname{T} \exp \int_{0}^{t} \left(-\frac{i}{\hbar}\right) \mathcal{H}(s) ds$$

$$= 1 - \frac{i}{\hbar} \int_{0}^{t} ds_{1} \mathcal{H}(s_{1}) - \frac{1}{\hbar^{2}} \int_{0}^{t} ds_{1} \int_{0}^{s_{1}} ds_{2} \mathcal{H}(s_{1}) \mathcal{H}(s_{2}) + \cdots$$
(A.2)

When we break up the present spin-boson Hamiltonian into three parts as

$$\mathcal{H}(t) = \mathcal{H}_{S}(t) + \mathcal{H}_{B} + \mathcal{H}_{I} \tag{A.3}$$

with

$$\mathcal{H}_{S}(t) = -\frac{1}{2}\hbar\delta\sigma^{x} - \frac{1}{2}H(t)\sigma^{z}, \quad \mathcal{H}_{B} = \sum_{\alpha}\hbar\omega_{\alpha}\left(n_{\alpha} + \frac{1}{2}\right),$$

$$\mathcal{H}_{I} = \sum_{\alpha}V_{\alpha}\sigma^{z}(b_{\alpha}^{\dagger} + b_{\alpha}), \tag{A.4}$$

the second-order approximant $U_2(t + \Delta t, t)$ to $U(t + \Delta t, t)$ for a small time step Δt is given [10] by

$$U_{2}(t + \Delta t, t)$$

$$= \exp\left[-\frac{i\Delta t}{2\hbar}\mathcal{H}_{S}\left(t + \frac{1}{2}\Delta t\right)\right] \exp\left(-\frac{i\Delta t}{2\hbar}\mathcal{H}_{B}\right) \exp\left(-\frac{i\Delta t}{\hbar}\mathcal{H}_{I}\right)$$

$$\times \exp\left(-\frac{i\Delta t}{2\hbar}\mathcal{H}_{B}\right) \exp\left[-\frac{i\Delta t}{2\hbar}\mathcal{H}_{S}\left(t + \frac{1}{2}\Delta t\right)\right], \tag{A.5}$$

i.e.,

$$U(t + \Delta t, t) = U_2(t + \Delta t, t) + O((\Delta t)^2). \tag{A.6}$$

Note that the partial Hamiltonian \mathcal{H}_{S} is evaluated at time $t + \frac{1}{2}\Delta t$; this is essential in constructing the second-order approximant to the time-ordered exponential [10]. Matrix elements of the approximate time-evolution operator are calculated in the same way as in the previous paper [11].

References

- [1] D. D. Awschalom, J. F. Smyth, G. Grinstein, D. P. DiVincenzo, and D. Loss, Phys. Rev. Lett. 68 (1992) 3092.
- [2] A. Garg, Phys. Rev. Lett. **71** (1993) 4249.
- [3] E. M. Chudnovsky, J. Appl. Phys. **73** (1993) 6697.
- [4] J. Tejada, X. X. Zhang, E. del Barco, J. M. Hernández, and E. M. Chudnovsky, Phys. Rev. Lett. 79 (1997) 1754.
- [5] S. Miyashita, J. Phys. Soc. Jpn. **65** (1996) 2734.
- [6] H. De Raerdt, S. Miyashita, K. Saito, D. Garcia-Pablos, and N. Garcia, Phys. Rev. B 56 (1997) 11761.
- [7] C. Zener, Proc. R. Soc. London A **137** (1932) 696.
- [8] D. P. Landau and E. M. Lifshitz, "Quantum Mechanics" third edition (Pergamon, Oxford, 1977) —S 90.
- [9] A. J. Leggett, S. Chakravarty, A. T. Dorsey, M. P. A. Fisher, A. Garg, and W. Zwerger, Rev. Mod. Phys. 59 (1987) 1.
- [10] M. Suzuki, Proc. Japan Acad. **69** Ser. B (1993) 161.
- [11] H. Kobayashi, N. Hatano, A. Terai, and M. Suzuki, Physica A 226 (1996) 137.
- [12] Y. Kayanuma and S. Fukuchi, J. Phys. B: At. Mol. Phys. 18 (1985) 4089.

Figure captions

- Figure 1: A schematic of the energy spectrum of the two-level system (1.1) (the solid line). The dashed lines denote the eigenvalues of the second term only. The labels $|\uparrow\rangle$ and $|\downarrow\rangle$ indicate the states in the limit $H \to \pm \infty$.
- Figure 2: The energy spectrum in the one-mode case (2.1). The abscissa is the magnetic field \tilde{H} . The labels $|\downarrow,0\rangle$ and $|\uparrow,n\rangle$ indicate the relevant physical interpretation of the states, where n is the number of excited bosons.
- Figure 3: The time evolution of the magnetization $\langle \sigma^z \rangle_{\tilde{t}}$ (dotted line) and the total energy $\tilde{E}(\tilde{t})$ (dashed line). The field was changed as $\tilde{H} = (1/500)\tilde{t}$. The ground-state energy for each value of \tilde{H} is also shown as the solid line.
- Figure 4: The time evolution of the magnetization $\langle \sigma^z \rangle_{\tilde{t}}$ (dashed line) and the energy of the spin, $\tilde{E}_{\rm spin}(\tilde{t}) \equiv \langle -\frac{1}{2}\tilde{\delta}\sigma^x \frac{1}{2}\tilde{H}(\tilde{t})\sigma^z \rangle_{\tilde{t}}$ (solid line).
- Figure 5: The time evolution of the eigenstate weights p_i . The solid line p_1 indicates the component of the ground state.
- Figure 6: The expectation value of the magnetization calculated from the Landau–Zener formula (solid line) for the case (2.1) with $\tilde{t}_{\text{max}} = 500$. The result is consistent with the numerical data of the magnetization if we average the data over the oscillations due to spin precession.
- Figure 7: The energy spectrum of the Hamiltonian with two boson modes: Case (i) $\tilde{\omega}_1 = 0.3$ and $\tilde{\omega}_2 = 0.35$. The abscissa is the magnetic field \tilde{H} .
- Figure 8: The time evolution of the magnetization $\langle \sigma^z \rangle_{\tilde{t}}$ (dotted line) and the total energy $\tilde{E}(\tilde{t})$ (dashed line) in the case (i) with $\tilde{v}=1/500$. The ground state energy for each value of \tilde{H} is also shown as a solid line.
- Figure 9: The time evolution of the probabilities p_i in the case (i) with $\tilde{v} = 1/500$.
- Figure 10: The energy spectrum of the Hamiltonian with two boson modes: Case (ii) $\tilde{\omega}_1 = 0.3$ and $\tilde{\omega}_2 = 0.31$.
- Figure 11: The time evolution of the eigenstate weights p_i in the case (ii) with $\tilde{v} = 1/500$.
- Figure 12: The time evolution of the magnetization $\langle \sigma^z \rangle_{\tilde{t}}$ (dotted line) and the total energy $\tilde{E}(\tilde{t})$ (dashed line) in the case (ii) with $\tilde{v} = 1/500$. The ground state energy for each value of \tilde{H} is also shown as a solid line.
- Figure 13: The estimates of the effective gaps $\Delta \tilde{E}^{(\text{eff})}$ (solid line), $\Delta \tilde{E}_{2}^{(\text{eff})}$

(dashed line), and $\Delta \tilde{E}_3^{(\text{eff})}$ (dotted line) for different values of \tilde{v} . The estimates barely depend on \tilde{v} .

Figure 14: The energy spectrum of the Hamiltonian with two boson modes: Case (iii) $\omega_1 = \omega_2 = 0.3$.

Figure 15: The time evolution of the eigenstate weights p_i in the case (iii) with $\tilde{v} = 1/500$. The weights p_3 , p_5 , p_6 , p_8 , and p_9 vanish for all \tilde{t} .

Figure 16: The time evolution of the magnetization $\langle \sigma^z \rangle_{\tilde{t}}$ (dotted line) and the total energy (dashed line) in the case (iii) with $\tilde{v} = 1/500$. The ground state energy for each value of \tilde{H} is also shown as a solid line.

Figure 17: The $\tilde{\omega}_2$ -dependence of the effective gaps. The difference between the solid line and the dashed line is $[\Delta \tilde{E}_1^{(\text{eff})}]^2$ and that between the dashed line and the dotted line is $[\Delta \tilde{E}_2^{(\text{eff})}]^2$. The combined energy gap for the two scattering points around $\tilde{H} \sim 0.3$ is given by Eq. (3.8), or the the dashed line.

Figure 18: The effective gap for the scattering points around $\tilde{H}=0.3$ and the real energy gaps near those scattering points. The solid line denotes the combined effective gap $(\Delta \tilde{E}^{(\text{eff})})^2$, the dashed line denotes the left-hand side of Eq. (3.3), $(\Delta \tilde{E}_2)^2 + (\Delta \tilde{E}_3)^2$, and the dotted line denotes $(\Delta \tilde{E}_2 + \Delta \tilde{E}_3)^2$.

- Fig. 1. A schematic of the energy spectrum of the two-level system
- Fig. 2. The energy spectrum in the one-mode case (2.1). The abscissa is the magnetic field \tilde{H} . The labels $|\downarrow,0\rangle$ and $|\uparrow,n\rangle$ indicate the relevant physical interpretation of the states, where n is the number of excited bosons.
- Fig. 3. The time evolution of the magnetization $\langle \sigma^z \rangle_{\tilde{t}}$ (dotted line) and the total energy $\tilde{E}(\tilde{t})$ (dashed line). The field was changed as $\tilde{H} = (1/500)\tilde{t}$. The ground-state energy for each value of \tilde{H} is also shown as the solid line.
- Fig. 4. The time evolution of the magnetization $\langle \sigma^z \rangle_{\tilde{t}}$ (dashed line) and the energy of the spin, $\tilde{E}_{\rm spin}(\tilde{t}) \equiv \langle -\frac{1}{2}\tilde{\delta}\sigma^x \frac{1}{2}\tilde{H}(\tilde{t})\sigma^z \rangle_{\tilde{t}}$ (solid line).
- Fig. 5. The time evolution of the eigenstate weights p_i . The solid line p_1 indicates the component of the ground state.
- Fig. 6. The expectation value of the magnetization calculated from the Landau–Zener formula (solid line) for the case (2.1) with $\tilde{t}_{\rm max}=500$. The result is consistent with the numerical data of the magnetization if we average the data over the oscillations due to spin precession.
- Fig. 7. The energy spectrum of the Hamiltonian with two boson modes: Case (i) $\tilde{\omega}_1 = 0.3$ and $\tilde{\omega}_2 = 0.35$. The abscissa is the magnetic field \tilde{H} .
- Fig. 8. The time evolution of the magnetization $\langle \sigma^z \rangle_{\tilde{t}}$ (dotted line) and the total energy $\tilde{E}(\tilde{t})$ (dashed line) in the case (i) with $\tilde{v} = 1/500$. The ground state energy for each value of \tilde{H} is also shown as a solid line.
- Fig. 9. The time evolution of the probabilities p_i in the case (i) with $\tilde{v} = 1/500$.
- Fig. 10. The energy spectrum of the Hamiltonian with two boson modes: Case (ii) $\tilde{\omega}_1=0.3$ and $\tilde{\omega}_2=0.31$.
- Fig. 11. The time evolution of the eigenstate weights p_i in the case (ii) with $\tilde{v} = 1/500$.
- Fig. 12. The time evolution of the magnetization $\langle \sigma^z \rangle_{\tilde{t}}$ (dotted line) and the total energy $\tilde{E}(\tilde{t})$ (dashed line) in the case (ii) with $\tilde{v} = 1/500$. The ground state energy for each value of \tilde{H} is also shown as a solid line.
- Fig. 13. The estimates of the effective gaps $\Delta \tilde{E}^{(\text{eff})}$, $\Delta \tilde{E}_2^{(\text{eff})}$ and $\Delta \tilde{E}_3^{(\text{eff})}$ for different values of \tilde{v} . The estimates barely depend on \tilde{v} .
- Fig. 14. The energy spectrum of the Hamiltonian with two boson modes: Case (iii) $\omega_1 = \omega_2 = 0.3$.
- Fig. 15. The time evolution of the eigenstate weights p_i in the case (iii) with $\tilde{v} = 1/500$. The weights p_3 , p_5 , p_6 , p_8 , and p_9 vanish for all \tilde{t} .

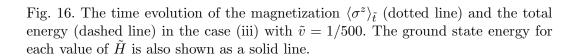


Fig. 17. The $\tilde{\omega}_2$ -dependence of the effective gaps.

Fig. 18. The effective gap for the scattering points around $\tilde{H}=0.3$ and the real energy gaps near those scattering points.

